Results in Chemistry 16 (2025) 102452

Contents lists available at ScienceDirect

Results in Chemistry

journal homepage: www.sciencedirect.com/journal/results-in-chemistry

Bio-based graphene-coated Co@CS catalysts are used to selectively hydrogenate nitriles to prepare primary amines via flow synthesis under mild conditions☆

Siyi Mi [a,b], Jianguo Liu [b,*]

[a] Southeast University-Monash University Suzhou Joint Graduate School, Southeast University, Suzhou 215000, China
[b] School of Energy and Environment, Southeast University, Nanjing 210096, China

ARTICLE INFO

Keywords:
Continuous hydrogenation
Reductive amination
Benzonitrile
Bio-based heterogeneous catalyst

ABSTRACT

Amines are basic components of bioactive compounds, natural products, drugs, and functional materials. Catalytic hydrogenation of nitrile compounds to corresponding amines is a green and efficient production method. Compared with heterogenous metal catalyzed batch reactions in high pressure of hydrogen, the flow synthesis method using heterogeneous metal catalysts can achieve higher catalyst efficiency and productivity, as well as much safer practical application. Moreover, the development of multiple utilizations of sustainable biomass materials especially in developing biobased materials for catalysts is highly demanding. So in this work, advanced flow synthesis methodology was used to prepare primary amines via bio-based chitosan Co@CS heterogeneous catalyst through the catalytic hydrogenation of nitrile. The effects of temperature, pressure, ammonia concentration, and liquid flow rate on the flow reaction were investigated. Under the optimal reaction conditions, the benzonitrile (BN) conversion rate was greater than 99 %, and the selectivity of benzylamine exceeded 99 %. The synthesized graphene-encapsulated Co-based catalyst with chitosan as the carrier material was tested for a long time to verify the stability of the Co@CS catalyst. The substrate expansion experiments of various aromatic nitriles gave satisfactory primary amine yields. Due to its exceptional mass and heat transport properties, the H-Flow system offers an efficient route for the large-scale synthesis of primary amines from biomass platform compounds in industrial production. This study provides new ideas and references for preparing highly selective primary amines by industrial-scale hydrogenation of nitrile compounds.

1. Introduction

Amines are key intermediates in the chemical industry. Due to their nucleophilic properties, they impart high reactivity [1]. Various amines, including primary, secondary, and tertiary amines, are widely used to produce agrochemicals, pharmaceuticals, dyes, and polymers [2]. Primary amines, in particular, are important raw materials for manufacturing drugs, pesticides, emulsifiers, and plasticizers [3]. Currently, the methods for synthesizing primary amines include reductive amination of carbonyl compounds [4], hydrogenation of nitro compounds [5], amination of alcohols [6], reduction of nitrile compounds [7], and N-alkylation of halogenated compounds [8]. Among them, the catalytic hydrogenation of nitrile compounds using molecular hydrogen as a reducing agent has the advantages of high atom economy [9] and a simple process and is a popular choice for the industrial synthesis of amine compounds [10]. However, nitrile hydrogenation also has disadvantages. The hydrogenation mechanism is complex as shown in Fig. 1. The by-products include partially hydrogenated nitrile compounds, also known as imines, and condensation side reactions with other nucleophilic substances such as substrates in the hydrogenation system to form secondary and tertiary amines [11], resulting in the problem of low selectivity of the amination product in the reaction [12]. It is still a huge challenge to obtain primary amines with high selectivity.

Precious metals such as Ru [13], Pd [14], Pt [15], Re [16], etc. are more commonly used in nitrile hydrogenation reduction and some heterogeneous catalysts have superior conversion effects [17]. However, the scarcity and high cost of precious metals hinder their widespread industrial application, while transition metals [18], which are more

☆ This article is part of a Special issue entitled: 'Organic Chemistry' published in Results in Chemistry.

* Corresponding author.
E-mail address: liujg@seu.edu.cn (J. Liu).

https://doi.org/10.1016/j.rechem.2025.102452
Received 5 April 2025; Received in revised form 12 June 2025; Accepted 13 June 2025
Available online 14 June 2025

abundant in earth resources and have lower costs, have come into the public eye [19]. Homogeneous catalytic systems including Co-, Fe- [20], and Mn-complexes show good selectivity under mild conditions and are of great interest to researchers [7]. Bornschein's team [20] was the first to use the iron PNP clamp complex to achieve good functional group tolerance. Esters, ethers, acetamidobenzenes, and amino substituents were not reduced in the presence of nitriles. The complex developed by the team constituted the first example of homogeneous catalysis, successfully achieving the selective hydrogenation of industrially important dinitriles to 1,6-hexane diamine. Mukherjee's team [21] first reported a reaction case catalyzed by Co PNNH clamp complexes to produce primary amines selectively. Elangovan's team [22] first described the use of manganese clamp complexes in the catalytic hydrogenation of nitriles, ketones, and aldehydes. However, metal contamination and recycling issues of these catalytic systems limit their commercial development and large-scale utilization. In heterogeneous catalytic systems, metal catalysts such as Ni [23] and Co [24] usually hydrogenate nitrile compounds under harsh conditions [25]. From the perspective of green chemistry and sustainable development, it is of great significance to develop non-precious metal catalysts that can show high activity under mild conditions [26].

Carbon-encapsulated non-precious metal catalysts have become a hot topic of research in recent years due to their special morphology, structure and electronic properties. It is a structure of metal core@carbon shell formed by encapsulating carbon materials on the surface of metal nanoparticles [27]. Due to the presence of carbon shells on the surface, carbon-encapsulated catalysts can not only avoid oxidation, migration, agglomeration and loss of metal particles during catalytic reactions, but also effectively prevent metal particles from being corroded by acid, greatly improving the stability of the catalyst [28]. In addition, when the metal active components are encapsulated, the activity and selectivity of the catalyst will also change significantly due to the influence of the geometric structure and electronic properties of the carbon shell, which makes carbon-encapsulated non-precious metal catalysts have broad application value and prospects in the field of catalytic hydrogenation [29].

Recently, much more fit for the above requirements of green chemistry and sustainable development, the advanced flow synthesis methodology attracted more and more attention. The continuous flow technology can better control process parameters [30], improve mass transfer and heat transfer [31], shorten reaction time [32], improve reaction safety [33], and make up for the shortcomings of traditional intermittent reactors in many aspects such as low production capacity and difficult catalyst separation [34]. Due to the limitation of microchannels and the dominant role of capillary forces [35], the gas-liquid flow in micro-packed bed reactors differs from that in kettle reactors [36]. The gas-liquid contact is more complete at the microscale, and the mass transfer performance is 1–2 orders of magnitude higher, which is conducive to the high selectivity of target products [37]. To the best of our knowledge, there are still limited reports on the hydrogenation of nitriles via bio-based Co heterogeneous catalyst in continuous flow.

Our group has been working on developing bio-based graphene-encapsulated no-precious metal catalysts for the synthesis of amines [38]. Previously, using biomass platform compounds citric acid, we prepared the bio-based graphene encapsulated Ni and Co heterogeneous catalysts and successfully applied them in the reductive amination of aldehydes in a batch reactor [39]. We also noticed that chitosan, another more abundant biomass platform compound, has been used as catalyst support. However, to our knowledge, a simple and practical preparation of the bio-based chitosan graphene-encapsulated Co catalyst and its utilization in the hydrogenation of nitriles through flow synthesis has not been reported yet. So, herein, for the first time, we used chitosan as the bio-based material to prepare the bio-based graphene-encapsulated Co catalysts and evaluated its reactivity in the hydrogenation of nitriles in an advanced automatic flow reactor. We optimized the process in a micro-packed bed reactor and verified the catalytic effect in a series of aromatic nitrile compounds. After long-term reaction tests, we found that the catalyst was well stable and did not lose reactivity significantly, which provides ideas for the subsequent continuous hydrogenation of nitriles to prepare primary amines in industrial production.

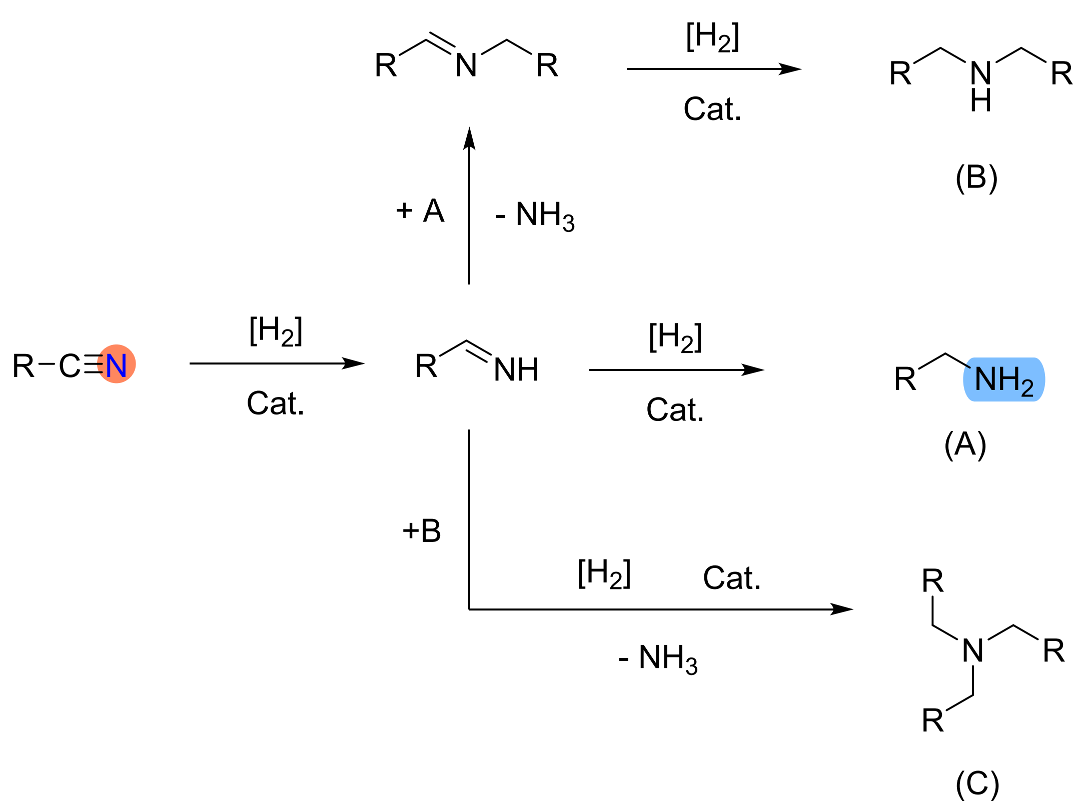

Fig. 1. General reaction mechanism of nitrile hydrogenation.

2. Experimental

2.1. Chemicals

Benzonitrile (C_7H_5N, 99 %), benzylamine (C_7H_9N, 99 %), N-benzylbutylamine ($C_{14}H_{13}N$, 95 %), dibenzylamine ($C_{14}H_{15}N$, 98 %), 3-cyanopyridine ($C_6H_4N_2$, 98 %), pyridine ($C_6H_8N_2$, 99 %), 1-naphthonitrile ($C_{11}H_7N$, 99 %), 1-naphthomethylamine ($C_{11}H_{11}N$, 98 %), 4-Methylthiocyanobenzene ($C_8H_7N_S$, 98 %), 4-methylthiobenzylamine ($C_8H_{11}NS$, 98 %), 4-tert-butylBN ($C_{11}H_{13}N$, 98 %), 4-tert-butylbenzylamine ($C_{11}H_{17}N$, 98 %), *p*-trifluoromethylBN ($C_8H_4F_3N$, 99 %), and *p*-trifluoromethylbenzylamine ($C_8H_8F_3N$, 98 %), N-(4-Cyanophenyl)acetamide ($C_9H_8N_2O$, 97 %), N-(4-(aminomethyl)phenyl)acetamide ($C_9H_{12}N_2O$, 95 %), 3,4-DimethoxyBN ($C_9H_9NO_2$, 98 %), 1-(3,4-Dimethoxyphenyl)methanamine ($C_9H_{13}NO_2$, 98 %), Terephthalonitrile ($C_8H_4N_2$, 98 %), 1-(3,4-1,4-Phenylenedimethanamine ($C_8H_{12}N_2$, 99 %), 1H-Indole-5-carbonitrile ($C_9H_6N_2$, 97 %), (1H-indol-5-yl)methanamine ($C_{10}H_{10}N_2$, 95 %), Quinoline-6-carbonitrile ($C_{10}H_6N_2$, 95 %), quinolin-6-ylmethanamine ($C_{10}H_{10}N_2$, 95 %) were purchased from Shanghai Merrill Chemical Technology Co., Ltd. Chitosan (deacetylation degree ≥95 %, viscosity 100–200 mPa·s), microcrystalline cellulose (100–200 mesh) and commercially available 10 % Pd/C and 5 % Ru/C catalysts were purchased from Shanghai MacLean Biochemical Co., Ltd. Co $(NO_3)_2\cdot 6H_2O$ (AR, 98 %) and methanol (CH_3OH, AR, 99.5 %) were from Sinopharm Chemical Reagent Co., Ltd. Ammonia (NH_3, 2/4/7 M in MeOH, safety seal) was from Shanghai Energy Chemical Co., Ltd. Hydrogen (H_2, 99.9 %) and nitrogen (N_2, 99.9 %) were supplied by Nanjing Ruier Special Gas Co., Ltd.

2.2. Synthesis of catalyst

This catalyst was synthesized using a simplified three-step procedure based on our previous work [40]. In 80 mL of anhydrous ethanol, dissolve cobalt (II) nitrate hexahydrate and chitosan at a molar ratio of 1:1. After agitating and aging the combination for four hours at 70 °C and 300 rpm to produce a rose-red suspension, the mixture was placed in an overnight drying oven at 100 °C to eliminate any remaining solvent. It was pounded in a mortar into a powder once it completely dried. The powder was next calcined for three hours at 600 °C in a tube furnace with a 50 ml/min high purity N_2 atmosphere and a temperature rise rate set at 5 °C/min. Then the catalyst is known as Co@CS, in a comparable manner non-nitrogen-doped carbon materials were created by calcining microcrystalline cellulose as the raw material, and the resulting cobalt-based catalyst was given the name Co@MC. The other operations were the same, and the material after calcination with only chitosan added but no cobalt-based precursor was named CS.

2.3. Material characterization

Catalyst morphology was observed using scanning electron microscopy (SEM), performed on an analytical SEM Inspect F50 (FEI, U.S.A.) microscope operating at a voltage of 10 kV. Transmission electron microscopy (TEM) analysis of catalyst surface loading was performed on a JEM-2100F microscope (JEOL, Japan) with an operating voltage of 200 kV and an energy spectroscopy model of Oxford 80 T. X-ray diffractometer (XRD) was used to scan and analyze the prepared catalyst powder to obtain the diffraction pattern. Cu Kα radiation was used, the voltage was 40 kV, the current was 20 mA (λ = 1.5406 Å), and the conventional angle was selected, that is, 5–80° (5°/min), and compared to the powder diffraction file (PDF) database of the International Center for Diffraction Data (ICDD) for data processing. X-ray photoelectron spectroscopy (XPS) analysis of metal valence states was performed on an Escalab250 Xi photoelectron spectrometer (Thermo Scientific Nexsa, USA). Brunauer-Emmett-Teller (BET) surface area and pore volume of nanocomposites were measured on an ASAP-2460 (Quantachrome, U.S.A.). The pore size distribution was obtained using the Barrett-Joyner-Halenda (BJH) method. Raman spectroscopy (Raman) was tested using an Xplora Plus intelligent fully automatic Raman spectrometer (HORIBA FRANCE SAS, France). A Nicolet IS50 (Thermo Fisher Scientific, China) Fourier transform infrared spectrometer (FT-IR) was used to evaluate the possible presence of functional groups in the samples.

2.4. Hydrogenation of benzonitrile in a flow reactor

A continuous flow reactor was used to perform the hydrogenation of the nitrile process (Ou Shi Sheng (Beijing) Technology Co., Ltd). The material was controlled by a plunger pump at a specific flow rate (0–9.99 mL/min) and pumped into a packed bed reactor. The flow rates of H_2 and N_2 gases were determined by a mass flow controller, with a flow rate of 0–100 sccm and a maximum pressure of 7.0 MPa. The reaction tube in the reactor was made of stainless steel, with a length of 25 cm, an inner diameter of 4.1 mm, and an outer diameter of 6.3 mm. The mixed liquid after the reaction flowed through the gas-liquid separator at a constant flow rate. After at least three liquid residence times and the micro-filling platform remained stable, samples were collected, the reaction products were identified using a gas chromatograph GC-2014C (Shimadzu, Japan), and the yield of the corresponding target product was calculated. Subsequently, solvent and nitrogen were flushed in to replace the remaining reactants. After the experiment, the system pressure was reduced and the temperature was cooled.

The liquid phase products were analyzed using GC equipped with a capillary chromatography column (HP-5, 30 m × 250 mm × 0.25 μm) and a flame ionization detector (FID). The temperature program is set as follows: injection temperature is 260 °C, the column temperature is maintained at 50 °C for 2 min and then raised to 250 °C at a heating rate of 5 $^{\circ}C\cdot min^{-1}$ and maintained at this temperature for 3 min, the detector temperature is 280 °C. Methanol is a solvent. The injection volume: 1 μL. The separation ratio is 20: 1.

3. Results and discussion

3.1. Catalyst characterization

The graphene shell nanoparticle catalyst was analyzed in detail by SEM (Fig. 2a). As expected, the nitrogen-doped carbon material showed obvious sponge-like porous characteristics, with highly ordered and regular carbon sheet structure and identifiable pores. According to the TEM image (Fig. 2b), the metal nanoparticles were well dispersed on the surface of the carbonaceous matrix, and the EDS spectrum (Fig. 2c-f) also visually verified that the C, N, O, and Co elements were highly dispersed in the catalyst. The chitosan carrier contains rich N/O functional groups, porous structure, and large specific surface area, which can anchor the Co nanoparticles more tightly and provide abundant adhesion sites for the Co nanoparticles so that the Co nanoparticles have good dispersion and promote the high activity of the catalyst. It is not difficult to find well-resolved stripes with a spacing of 0.204 nm on the metal nanoparticles through the polycrystalline selected area electron diffraction rings, which corresponds to the formation of the Co (111) plane during the pyrolysis process, and the crystal plane corresponds to the grating number.

XRD is widely used to determine the crystal structure in carbonaceous materials, while Raman spectroscopy has also been established as a complementary technique for probing the microstructure of carbonaceous supports based on structural parameters calculated by XRD. Both of these two tests work synergistically to provide structural information on Co@CS catalysts. The XRD spectrum (Fig. 3a) shows that the peak at 20.16° can be attributed to the typical characteristic peak of chitosan, while strong diffraction peaks appear at 2θ = 44.216, 51.522, and 75.853, which correspond to the crystal (111), (200), and (220) planes of Co, respectively, indicating that metallic cobalt has been successfully loaded on the chitosan support. Combined with Raman spectroscopy (Fig. 3b), the two characteristic Raman peaks at 1343 cm^{-1} and 1571

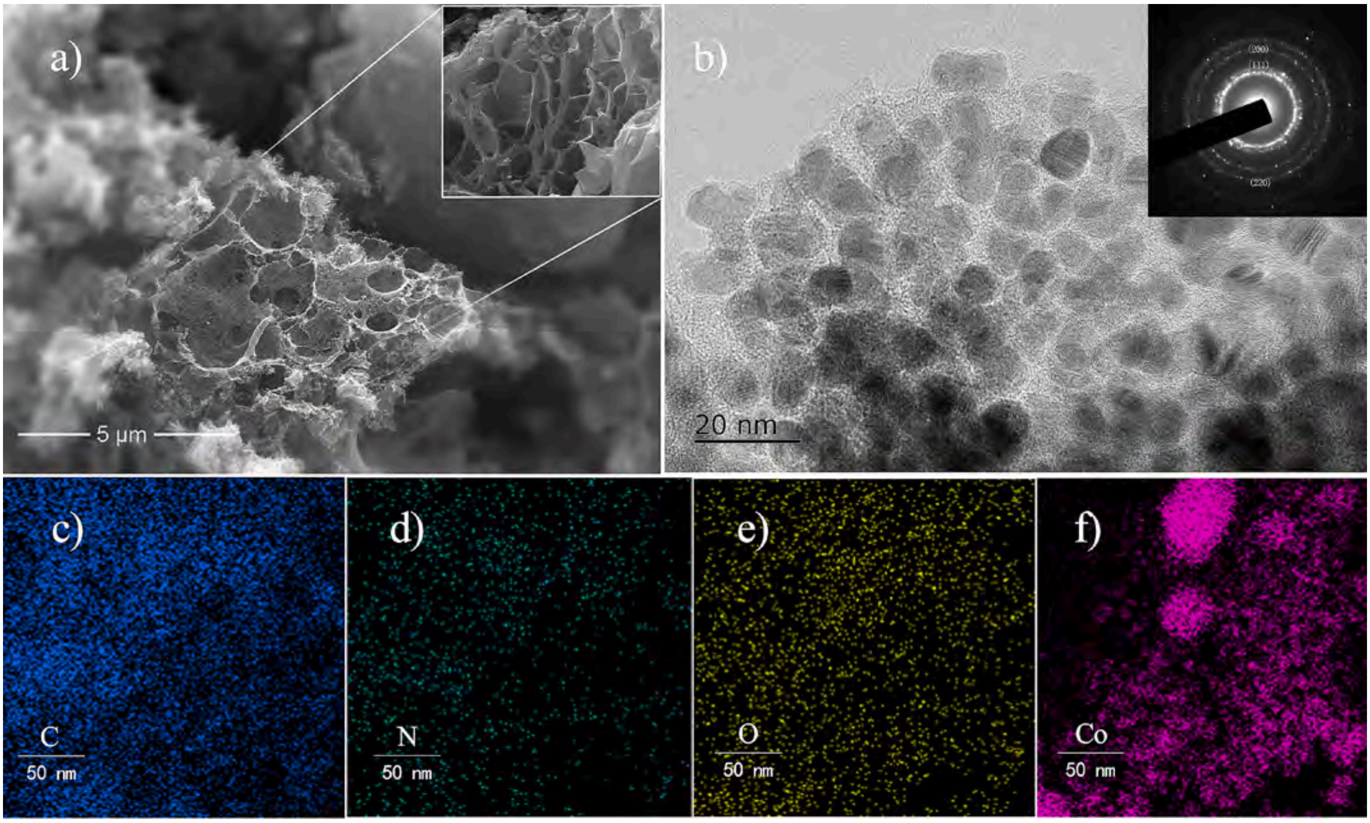

Fig. 2. SEM (a) and TEM (b) and EDS element mapping of C, N, O, and Co (c-f) images of the Co@CS catalyst.

cm^{-1} can be attributed to the D band and G band, which are related to disordered carbon and sp^2 hybridized graphitic carbon structures, respectively. The intensity ratio (I_D/I_G) represents the degree of graphitization and disorder of the carbon material. The I_D/I_G value of Co@CS is higher than that of the carrier CS, indicating that there are more defect sites due to the introduction of Co substance.

Combined with FT-IR spectroscopy (Fig. 3c), it is shown that there are acidic functional groups on the catalyst surface, among which the characteristic peaks of hydroxyl and carboxyl groups indicate that there are sufficient acid sites for the catalytic process. The introduction of metal Co in the Co@CS catalyst can act as a Lewis site with moderate acidity, promoting the breaking of the C—O bond. The -NH-C=O bond at 1631.001 cm^{-1} also confirms the presence of N in the catalyst. Subsequently, the elemental composition and valence state of the Co@CS sample were further analyzed by XPS. According to the energy spectrum (Fig. 3d-g), C, N, O, and Co elements are present in the catalyst. For the C 1 s orbital spectrum, the peak with a binding energy of 284.8 eV comes from the sp^2 C hybridization of graphene, indicating the formation of a graphitic carbon structure encapsulating metal atoms. The remaining binding energies at 285.92, 287.52, 289.37, and 292.20 eV correspond to C—N, C—O, C═O, and C(O)OH, respectively. Among them, the peak at 284.80 eV is the most important, representing the degree of graphitization of the catalyst. The peak at 285.92 eV is attributed to C—N, emphasizing the presence of N in the sample. The Co functional group characteristic peak is located in the range of 778–783 eV, corresponding to a specific form of Co^0 and Co^{2+}, namely CoO and $Co(OH)_2$, and the oscillation satellite peak of the Co element is at 785.80 eV. For the N 1 s spectrum, the nitrogen species in the carbon element are mainly composed of the following: pyridinic nitrogen (398.57 eV), amino group (399.95 eV), pyrrolic N (400.87 eV), graphitic N (402.92 eV) and nitrogen oxides (406.13 eV), which is consistent with the catalyst component also using chitosan as carrier. BET characterization results (Fig. 3h-i) further illustrate that these N-doped carbon supports show high surface area and mesoporous structure. According to the N_2 adsorption-desorption isotherm, a typical IV-type isotherm with an H-3 type hysteresis loop appears, indicating that the Co@CS catalyst forms a porous structure during pyrolysis. These carbon materials are composed of nanosheets with uniform size and shape of cracks or pores, which is consistent with the SEM image observation. The specific surface area of Co@CS obtained by using the adsorption isotherm is 198.82 m^2/g, the total pore volume is 0.215 cm^3/g, and the average pore size is 5.576 nm. The larger specific surface area after calcination may be due to the richer pore structure produced by the partial carbonization of the material. The large surface area is conducive to providing abundant active centers for the catalytic reaction and facilitating the transport of reactants and products in the channel.

3.2. *Effect of factors*

3.2.1. *Catalyst screening*

Catalysts are important factors affecting the hydrogenation of nitrile compounds. The type and preparation method of catalysts plays a crucial role in the selectivity of the reaction. Therefore, we first tested the effects of different catalysts on the catalytic hydrogenation of BN in a batch reactor, evaluated the six selected catalysts, and the yields of the target products are summarized in Fig. 4. Obviously, the effects of the two commercially available catalysts are far from satisfactory. For the Pd/C catalyst, the substrate conversion can be fully carried out, but the selectivity for benzylamine (BA) is only 43.49 %, and the remaining products include dibenzylamine, toluene and a small amount of benzyl alcohol. For the Ru/C catalyst, we detected a large amount of residual BN in the reaction solution, and the conversion rate was only 45.32 %. The target product showed a high selectivity of 99.25 %, and the rest was N-benzylbutylamine. The amination ideas reported in the past literature were all completed under the catalysts of Raney Ni [41], but considering that Raney Ni itself is extremely prone to spontaneous

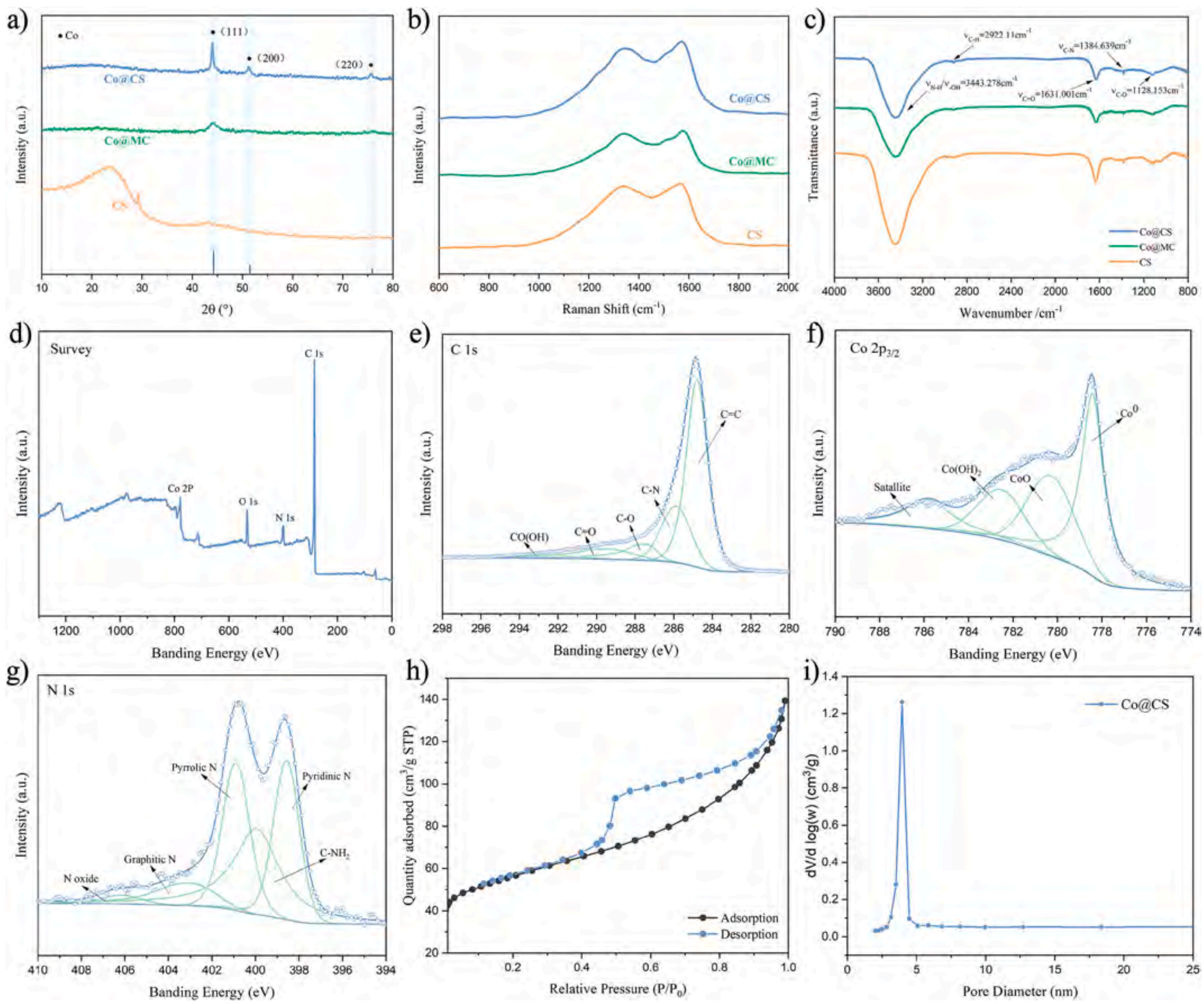

Fig. 3. a) XRD results, b) Raman spectra, c) FT-IR spectra of selected catalytic materials, d-g) XPS images, h-i) N_2 adsorption-desorption isotherm of Co@CS with its survey.

combustion when in contact with air [42], it is highly dangerous and is not used in this experiment. Then, we replaced Raney nickel with the developed graphene-encapsulated Ni-based catalyst [39a] to hydrogenate BN. Unlike the effect of the above-mentioned precious metal catalysts, we could achieve 80.81 % conversion rate and 91.94 % selectivity on the Ni@C catalyst, indicating the feasibility of transition metal elements in the reaction of hydrogenation of nitrile to amine.

We then used the transition metal element Co in the catalytic reaction and used Co-based catalysts synthesized from different carrier materials as a control group to verify the catalytic effect. As shown in the graphic results, the product selectivity of nitrile hydrogenation is not only related to the properties of the metal species but also inseparable from the carrier. When using microcrystalline cellulose as a raw material, the non-nitrogen-doped catalyst Co@MC only gave a conversion rate of 74.14 % and a selectivity of 89.90 %, which is in contrast to the almost complete yield of the catalyst wrapped with the nitrogen-doped carrier chitosan, indicating that N-doping of the carbon carrier can significantly improve the catalytic activity. At the same time, we also used the empty carrier CS in the reaction for comparative experiments. It can be seen that almost no hydrogenation reaction occurs under the pure carrier catalyst, indicating that Co is an active substance that can carry out this reaction. Subsequently, we moved the reaction to a continuous flow micro-packed bed reactor to further optimize the reaction conditions.

3.2.2. *Effect of temperature*

In this section, we systematically tested the catalytic effect of the reaction in the range of 40–120 °C to explore the effect of temperature change on the hydrogenation reaction of BN. As shown in Fig. 5a, as the temperature increases from 40 °C to 80 °C, the substrate conversion rate increases from 80.89 % to >99 % respectively, and the selectivity gradually increases from 66.42 % to >99 %. Both benzylamine and dibenzylamine generated by the hydrogenation of BN can be further hydrogenated to form toluene. In this temperature test range, the selectivity of the byproduct toluene is low and almost negligible, proving that a suitable catalyst can effectively improve the selectivity of the target product.

3.2.3. *Effect of pressure*

We all know that the mass transfer of hydrogen on the catalyst surface is a key factor in controlling the reaction rate and is directly related to the hydrogen partial pressure. We then explored the effect of different

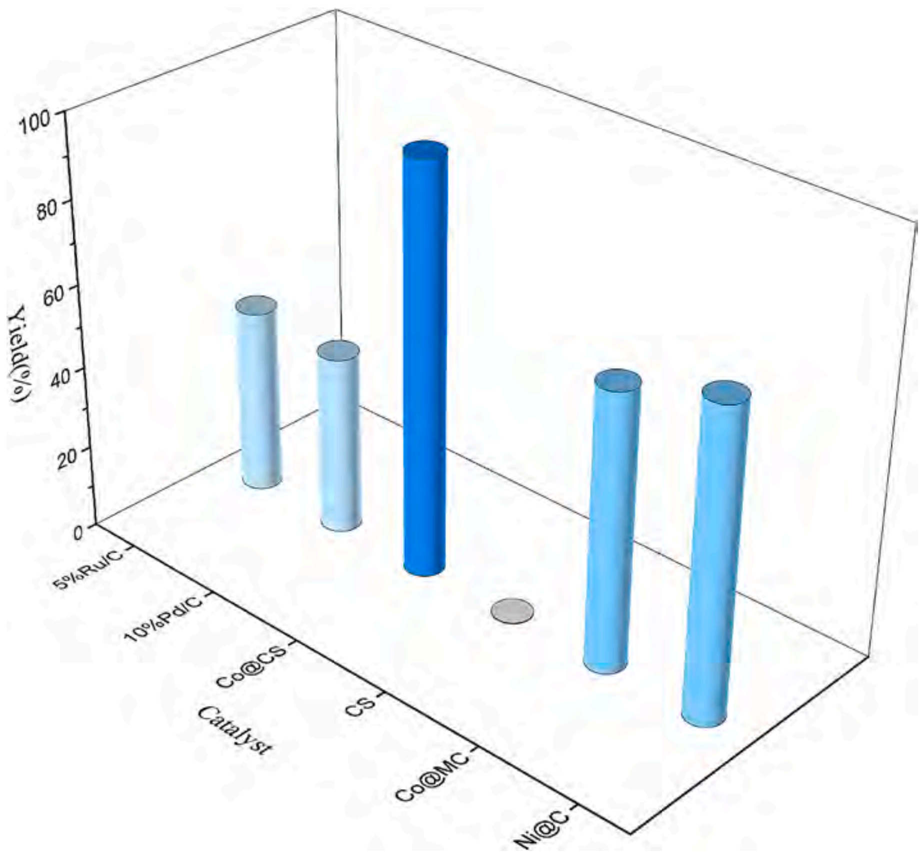

Fig. 4. The screening of prepared and commercial catalysts is based on the following conditions: 100 °C, 1 MPa, 4 h, 20 mg catalyst, 5 mL ammonia solution (7 M NH_3 in MeOH), and 0.5 mmol BN.

hydrogen pressures on the hydrogenation of BN (Fig. 5b). From the initial test of 0.5 MPa, the reaction showed a satisfactory yield. With the increase in pressure, the conversion rate and selectivity did not change significantly. We know that the mass transfer of hydrogen is not an absolute factor limiting the reaction rate. The reaction can proceed at a lower pressure, which lays a certain foundation for the hydrogenation of nitrile compounds under mild conditions in continuous flow.

3.2.4. Effect of NH_3 concentration

In the hydrogenation reaction, nitrile compounds not only generate the target product primary amine but also by-products secondary amine and tertiary amine. The benzylamine and dibenzylamine generated by the hydrogenation of BN discussed above can also continue to react to form toluene. To avoid the occurrence of side reactions, an alkali additive can be added to the reaction, and then the effect of ammonia concentration in the solution on the yield of benzylamine was tested. As shown in Fig. 5c, we first used pure methanol reagent as the reaction solvent, and only obtained a conversion rate of 20.33 % and a selectivity of 50.69 %, indicating the necessity of alkali additives for the reaction. As the concentration of ammonia in the methanol solution increases from 2 to 7 mol/L, especially, it can be intuitively seen that when the ammonia methanol is 7 mol/L, it has a significant effect on the improvement of the substrate conversion rate, which increases significantly from 34.19 % at 2 mol/L to >99 % at 7 mol/L. Then 7 mol/L ammonia methanol solution was decided as the solvent for subsequent condition exploration.

3.2.5. Effect of liquid flow rate

The liquid flow rate affects the residence time between the substrate and the catalyst by changing the liquid holdup in the micro-packed bed reactor. A residence time that is too short will easily lead to an increase in the selectivity of the reaction intermediates, and a long residence time will also reduce the productivity of the system to a certain extent. As shown in Fig. 5d, when we set the material through the reaction tube at a flow rate of 2.5 mL/min, most of the substrate remained unreacted and kept in the reaction liquid, and the BN conversion rate was only 42.06 %. When the flow rate was gradually reduced to give BN and the catalyst sufficient contact time, we observed that the conversion rate increased linearly until 0.5 mL/min when the substrate conversion was complete and the selectivity of the target product was ensured. We set the flow rate under this condition as the optimal contact time.

3.3. Stability of the catalyst

We loaded the Co@CS catalyst into the reaction tube of the micro-packed bed reactor and optimized the process conditions including temperature, pressure, flow rate, ammonia methanol concentration. The whole process lasted 30 h. At each stage of the process optimization, we monitored the instantaneous conversion rate and selectivity under steady-state conditions every few hours, and calculated the corresponding BA yield. In the first 7 h, the reaction temperature conditions were screened. Stages *i-ii* showed that the BA yield increased during the temperature increase from 40 °C to 80 °C. Subsequently, the hydrogen pressure conditions were optimized during the 7–15 h stage. The yield hardly changed during the decrease from 3 MPa to 0.5 MPa. Then, the liquid flow rate was controlled for 15–23 h. During the process of gradually increasing the fluid flow rate from 1.0 sccm to 2.5 sccm in stage *iii*, it was observed that the target amine yield gradually decreased. In the next 23–30 h, the concentration of 2 M ammonia methanol in stage *iv* was gradually increased to 4 M in state *v* at the optimal flow rate of 0.5 sccm, and the BA yield was still less than 40 %. When the concentration was increased to 7 M, the yield returned to the expected level.

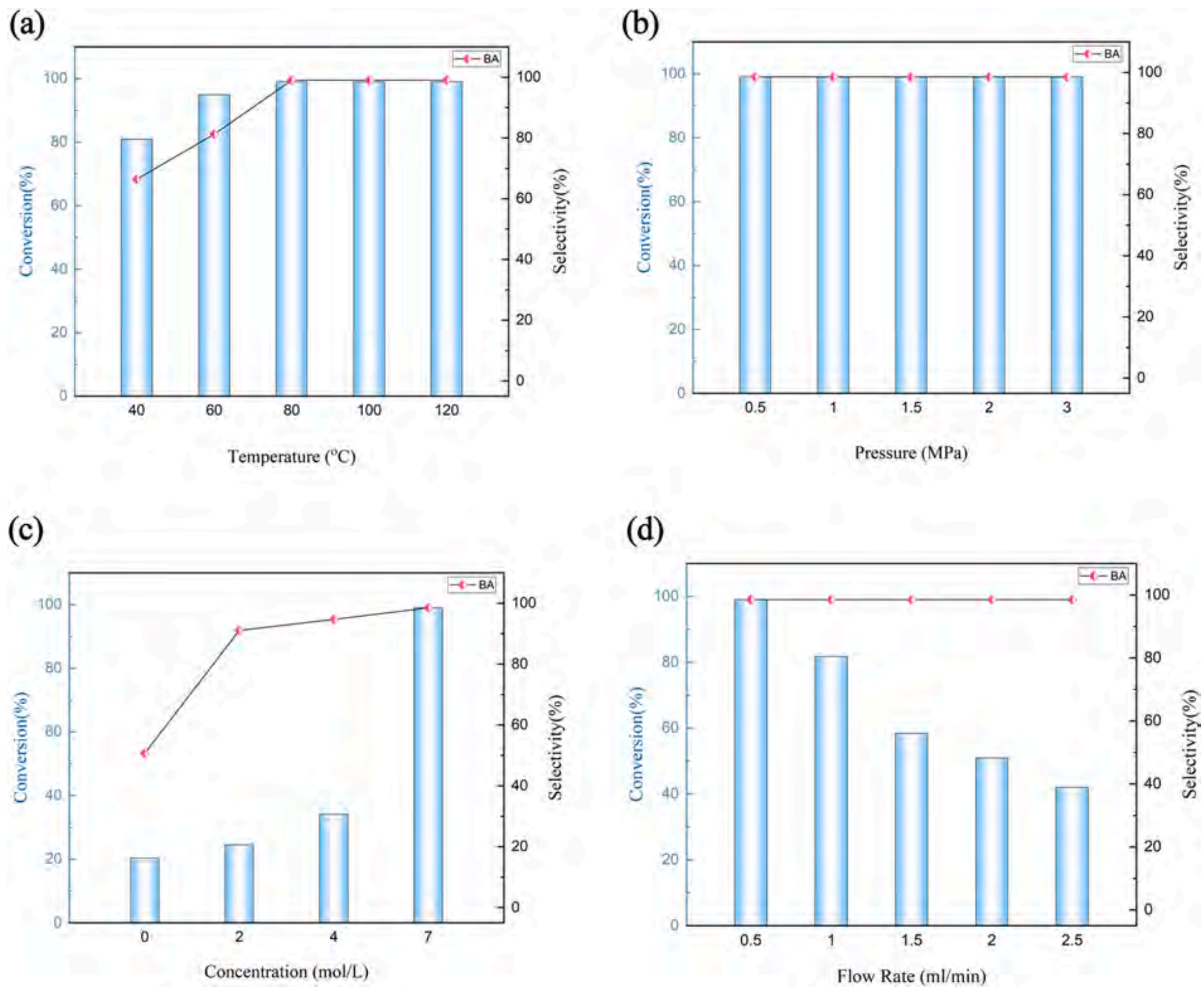

Fig. 5. BN continuous flow hydrogenation process. Reaction conditions: a) BN (0.1 mol/L), cat. (0.4 g), NH_3 (7 M in MeOH), H_2 pressure (3.0 MPa), liquid flow rate 0.5 mL/min. b) BN (0.1 mol/L), cat. (0.4 g), NH_3 (7 M in MeOH), temperature (80 °C), liquid flow rate 0.5 mL/min. c) BN (0.1 mol/L), cat. (0.4 g), NH_3, temperature (80 °C), H_2 pressure (0.5 MPa), liquid flow rate 0.5 mL/min. d) BN (0.1 mol/L), cat. (0.4 g), NH_3 (7 M in MeOH, temperature (80 °C), H_2 pressure (0.5 MPa).

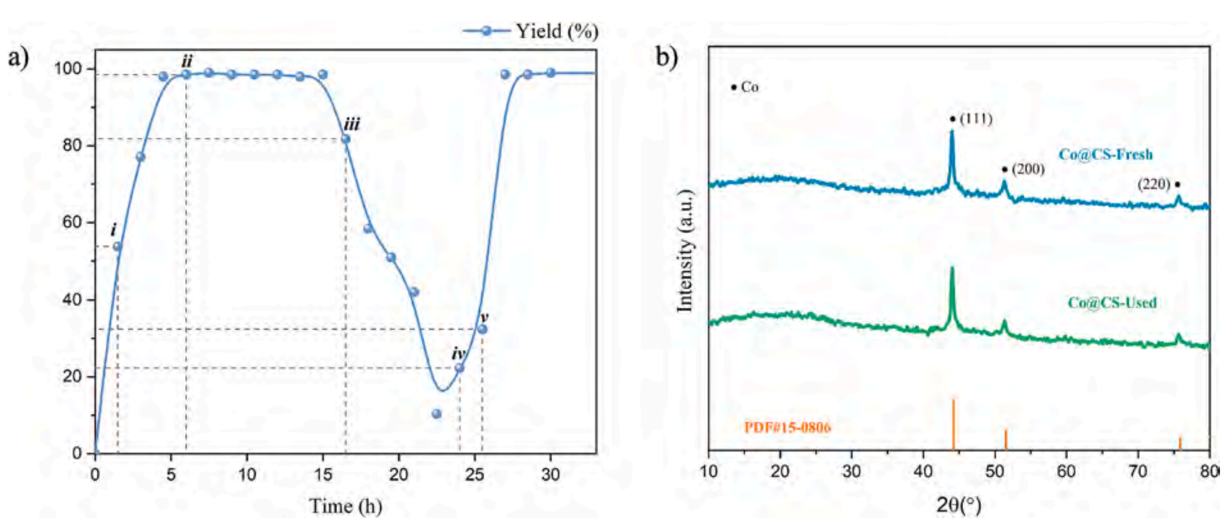

Fig. 6. a) Long-term reaction BN flow hydrogenation, reaction status: *i* (40 °C, 3 MPa H_2, 0.5 sccm, 7 M NH_3 in MeOH, 2.0 h), *ii* (100 °C, 3 MPa H_2, 0.5 sccm, 7 M NH_3 in MeOH, 7.0 h), *iii* (80 °C, 0.5 MPa H_2, 1.0 sccm, 7 M NH_3 in MeOH, 18 h), *iv* (80 °C, 0.5 MPa H_2, 0.5 sccm, 2 M NH_3 in MeOH, 24 h), *v* (80 °C, 0.5 MPa H_2, 0.5 sccm, 4 M NH_3 in MeOH, 26.0 h), b) XRD patterns of fresh and used Co@CS catalysts.

It is worth noting that during this process, the Co@CS catalyst was always loaded in the bed and was not taken out. After 30 h, the catalyst continued to run and maintained a high stability. After the long reaction test was completed, the catalyst was taken out for subsequent characterization. The XRD spectrum of the spent catalyst (Fig. 6b) shows that the carbon has a graphite structure and metallic cobalt is present, which indicates that the catalyst is still stable after a long reaction test. We were surprised that the catalytic system performed robustly in the long-term test, and the target product was harvested with excellent yields throughout the process. Moreover, the catalyst maintained excellent reactivity and product selectivity without losing activity significantly. Compared with traditional tank reactors, continuous flow technology can greatly shorten the reaction time, making it possible to synthesize primary amines on a kilogram scale per day or a ton scale per year, which further makes flow hydrogenation convenient and feasible for industrial production.

3.4. Mechanism study for the synthesis of primary amines

Studying reaction kinetics can help clarify the effect of temperature on the rate of chemical reactions to meet the needs of reaction process development and reactors [43]. The mass transfer resistance dissolved in the solution can be ignored [44]. However, it is still necessary to evaluate the mass transfer resistance brought about by the diffusion of substances to the outer surface of the catalyst, namely the external diffusion, and the mass transfer resistance accompanying the entry and exit of substances into the pore structure of the catalyst, namely the internal diffusion. According to previous literature reports [45], when the increase in the apparent velocity of the liquid does not affect the average reaction rate, it can be judged that the external diffusion is eliminated, and the external resistance has been eliminated in the same micro-packed bed reactor has been verified [46]. On the other hand, based on this theory, by calculating the Thiele modulus and efficiency factor, it can be seen that the internal mass transfer resistance is negligible for this kinetic experiment. The hydrogenation of BN can be regarded as a first-order reaction [47]. By optimizing the temperature conditions, it can be seen that the degree of hydrogenation has a good linear relationship with the temperature. The rate equation for the hydrogenation of benzene can be expressed as:

$$\mathrm{r} = -\frac{\mathrm{dC_{BN}}}{d\tau} = \mathrm{k_1 C_{BN}}$$

$$\mathrm{t} = \mathrm{t_0}, \mathrm{C_{BN}} = \mathrm{C_0}$$

$$\mathrm{t} = \tau, \mathrm{C_{BN}} = \mathrm{C_0}(1 - \mathrm{X})$$

$$k_1 = -\frac{\ln(1 - X)}{\tau}$$

From this we can know that the rate constant of the reaction can be calculated by the conversion rate of BN at different temperatures, and at the same time:

$$\tau = \frac{\pi \mathrm{D}^2 \mathrm{L} \varepsilon \mathrm{h}}{4\mathrm{F_l}}$$

Where D (cm) and L (cm) respectively represent the inner diameter and length of the reactor; ε is the porosity of the bed layer; F_l is the liquid flow rate; h is the liquid holding capacity.

Therefore, we selected the temperature range of 40–80 °C and tested the degree of hydrogenation of BN at 1 MPa H_2 and 0.8 mL/min. The conversion rate is shown in Fig. 7a. The yielded result was substituted into the reaction equation to calculate the reaction rate constant. Based on the linear fitting results of the Arrhenius equation, we obtained that the activation energy and exponential factor were 53.117KJ/mol and 19.495 s^{-1}, respectively.

3.5. Substrates expansions

To verify the universality of the Co@CS catalyst in the catalytic hydrogenation of nitrile compounds to synthesize primary amines, we expanded a variety of different nitriles in the continuous flow, including 3-polyamine and 1-naphthylamine (entries 1–2) for the production of pigments, dyes, and synthetic drug intermediates. As shown in Table 1, we noticed that when the temperature was raised to 120 °C and the pressure was 2 MPa, all aromatic nitriles and heterocyclic compounds showed a conversion rate greater than 99 %, and the formation of the corresponding primary amines showed high selectivity. The catalytic system is suitable for substrates containing halogen groups (entry 5), acetyl groups (entry 6), ether groups (entry 7), dinitriles (entry 8), and N-heterocyclic aromatic nitriles (entries 9–10). The hydrogenation by-products and self-coupling by-products were well suppressed, most nitrile compounds can be easily and selectively converted to their corresponding primary amines through this catalyst system. It demonstrates the applicability of graphene shell cobalt nanoparticles Co@CS as precursors for the selective preparation of amine-derived drugs in industrial applications.

4. Conclusion

A graphene-wrapped Co-based catalyst was successfully prepared by in-situ synthesis. The catalyst used chitosan, a biomass nitrogen source,

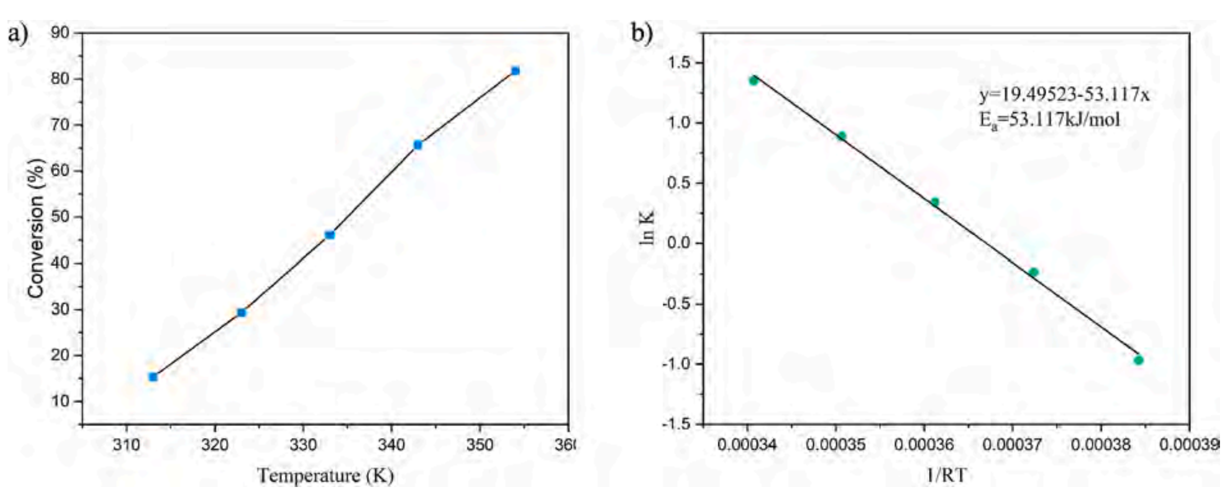

Fig. 7. a) Conversion of BN at different reaction temperatures b) Reaction conditions: BN (0.1 mol/L), cat. (0.4 g), NH_3 (7 M in MeOH), H_2 pressure (0.5 MPa), gas flow rate 40 sccm, liquid flow rate 0.8 mL/min.

Table 1
Hydrogenation of various nitriles by catalyst Co@CS.[a]

Entry	Substrate	Product	Temperature/°C	Pressure/MPa	Conv.(%)	Sel.(%)
1	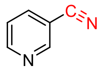	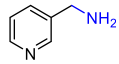	120	2	>99	98
2	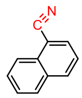	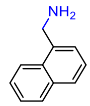	120	2	>99	96
3	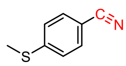	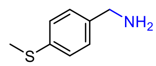	120	2	>99	92
4	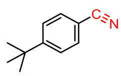	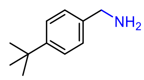	120	2	>99	98
5	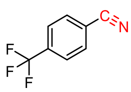	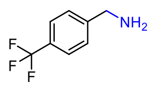	120	2	>99	97
6	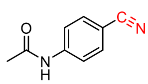	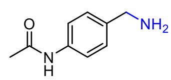	120	2	>99	93
7	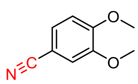	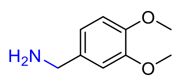	120	2	>99	91
8	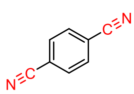	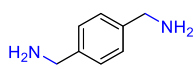	120	2	>99	97
9	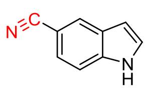	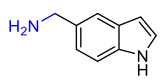	120	2	>99	94
10	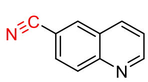	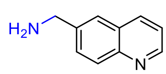	120	2	>99	93

[a] Reaction conditions: substrate (0.1 mol/L), 0.4 g catalyst, NH_3 in MeOH (7 mol/L), liquid flow 0.5 ml/min, 120 °C, H_2 Pressure 2.0 MPa. [b] Determined by gas chromatography with flame ionization detector (GC-FID); conversion of nitrile, Conv. (%); selectivity of the corresponding product, Sel. (%).

as a carrier material and was successfully applied in a continuous micro-packed bed reactor to hydrogenate BN to benzylamine. The effects of temperature, pressure, ammonia concentration, and the residence time of the material flowing through the reaction tube on the hydrogenation reaction were evaluated. At 80 °C, 0.5 MPa H_2, and a flow rate of 0.5 mL/min, the BN conversion rate and BA selectivity were higher than 99 %. The microreactor has excellent heat and mass transfer performance, and various aromatic nitriles were well tolerated under optimized conditions, and good yields were obtained under mild conditions. Surprisingly, within the kinetic range, the catalyst was subjected to a long-term catalyst stability test and the Co@CS catalyst showed no obvious deactivation phenomenon, showing excellent stability. This flow hydrogenation method uses nitrile as a simple and safe raw material to prepare primary amines, which is expected to become an efficient and practical synthetic route for various amine-containing functional materials. The continuous flow process also provides the possibility for industrial scale-up.

CRediT authorship contribution statement

Siyi Mi: Writing – original draft, Software, Resources, Methodology, Formal analysis, Data curation, Conceptualization. **Jianguo Liu:** Writing – review & editing, Visualization, Validation, Supervision, Project administration, Funding acquisition.

Declaration of competing interest

The authors declare that they have no known competing financial interests or personal relationships that could have appeared to influence the work reported in this paper.

Acknowledgment

This work was supported financially by the National Key Research and Development Program of China (2023YFD1701504).

Appendix A. Supplementary data

Supplementary data to this article can be found online at https://doi.org/10.1016/j.rechem.2025.102452.

Data availability

Data will be made available on request.

References

[1] V. Froidevaux, C. Negrell, S. Caillol, J.-P. Pascault, B. Boutevin, Chem. Rev. 116 (2016) 14181–14224.
[2] R.V. Jagadeesh, T. Stemmler, A.-E. Surkus, H. Junge, K. Junge, M. Beller, Nat. Protoc. 10 (2015) 548–557.

[3] V.G. Chandrashekhar, T. Senthamarai, R.G. Kadam, O. Malina, J. Kašlík, R. Zbořil, M.B. Gawande, R.V. Jagadeesh, M. Beller, Nat. Catal. 5 (2022) 20–29.
[4] K. Koh, U. Sanyal, M.S. Lee, G. Cheng, M. Song, V.A. Glezakou, Y. Liu, D. Li, R. Rousseau, O.Y. Gutiérrez, Angew. Chem. 132 (2020) 1517–1521.
[5] E. Kowalewski, K. Matus, A. Gajek, A Śrębowata in Catalytic Hydrogenation of Nitrocyclohexane with CuCo/SiO2 Catalysts in Gas and Liquid Flow Reactors 12, 2022.
[6] C. Gunanathan, D. Milstein, Angew. Chem. Int. Ed. 47 (2008) 8661–8664.
[7] J.A. Garduño, J.J. García, ACS Catalysis 10 (2020) 8012–8022.
[8] P. Ruiz-Castillo, S.L. Buchwald, Chem. Rev. 116 (2016) 12564–12649.
[9] S. Werkmeister, J. Neumann, K. Junge, M. Beller, *Chemistry – A* European Journal 21 (2015) 12226–12250.
[10] K. Murugesan, T. Senthamarai, M. Sohail, A.S. Alshammari, M.-M. Pohl, M. Beller, R.V. Jagadeesh, Chem. Sci. 9 (2018) 8553–8560.
[11] D.M. Sharma, B. Punji, Advanced Synthesis & Catalysis 361 (2019) 3930–3936.
[12] S. Chakraborty, H. Berke, ACS Catal. 4 (2014) 2191–2194.
[13] I.D. Alshakova, B. Gabidullin, G.I. Nikonov, ChemCatChem 10 (2018) 4860–4869.
[14] Y. Saito, H. Ishitani, M. Ueno, S. Kobayashi, ChemistryOpen 6 (2017) 211–215.
[15] S. Lu, J. Wang, X. Cao, X. Li, H. Gu, Chem. Commun. 50 (2014) 3512–3515.
[16] Z. Ma, L. Ma, X. Chen, X. Wang, Y. Tan, W. Yang, S. Wang, L. Yan, K. Zhu, Y. Ding, Chem. Eng. J. 466 (2023) 143238.
[17] H.-U. Blaser, C. Malan, B. Pugin, F. Spindler, H. Steiner, M. Studer, Adv. Synth. Catal. 345 (2003) 103–151.
[18] V.G. Chandrashekhar, W. Baumann, M. Beller, R.V. Jagadeesh, Science 376 (2022) 1433–1441.
[19] M. Sheng, S. Yamaguchi, A. Nakata, S. Yamazoe, K. Nakajima, J. Yamasaki, T. Mizugaki, T. Mitsudome, ACS Sustain. Chem. Eng. 9 (2021) 11238–11246.
[20] C. Bornschein, S. Werkmeister, B. Wendt, H. Jiao, E. Alberico, W. Baumann, H. Junge, K. Junge, M. Beller, Nat. Commun. 5 (2014) 4111.
[21] A. Mukherjee, D. Srimani, S. Chakraborty, Y. Ben-David, D. Milstein, J. Am. Chem. Soc. 137 (2015) 8888–8891.
[22] S. Elangovan, C. Topf, S. Fischer, H. Jiao, A. Spannenberg, W. Baumann, R. Ludwig, K. Junge, M. Beller, J. Am. Chem. Soc. 138 (2016) 8809–8814.
[23] J.A. Garduño, J.J. García, ACS Omega 2 (2017) 2337–2343.
[24] J. Long, K. Shen, Y. Li, ACS Catalysis 7 (2017) 275–284.
[25] T. Mitsudome, M. Sheng, A. Nakata, J. Yamasaki, T. Mizugaki, K. Jitsukawa, Chem. Sci. 11 (2020) 6682–6689.
[26] Z. Ma, V.G. Chandrashekhar, B. Zhou, A.M. Alenad, N. Rockstroh, S. Bartling, M. Beller, R.V. Jagadeesh, Chem. Sci. 13 (2022) 10914–10922.
[27] H. Mao, S. Peng, H. Yu, J. Chen, S. Zhao, F. Huo, J. Mater. Chem. A 2 (2014) 5847–5851.
[28] L. Tang, X. Meng, D. Deng, X. Bao, Adv. Mater. 31 (2019) 1901996.
[29] L. Yu, D. Deng, X. Bao, Angew. Chem. Int. Ed. 59 (2020) 15294–15297.
[30] S.D. Dempsey, A.A. Ryan, M. Smyth, T.S. Moody, S. Wharry, K. Fahey, A.M. Beale, S. Mediavilla Madrigal, P. Dingwall, D.W. Rooney, P.C. Knipe, M.J. Muldoon, J. M. Thompson, Reaction Chemistry & Engineering 8 (2023) 1559–1564.
[31] W.-J. Yoo, H. Ishitani, Y. Saito, B. Laroche, S. Kobayashi, J. Org. Chem. 85 (2020) 5132–5145.
[32] F. Ferlin, D. Lanari, L. Vaccaro, Green Chem. 22 (2020) 5937–5955.
[33] L. Leemans Martin, T. Peschke, F. Venturoni, S. Mostarda, Current Opinion in Green and Sustainable Chemistry 25 (2020) 100350.
[34] T. Yamada, K. Park, C. Furugen, J. Jiang, E. Shimizu, N. Ito, H. Sajiki, ChemSusChem 15 (2022) e202102138.
[35] J. Kobayashi, Y. Mori, S. Kobayashi, Chemistry – An Asian Journal 1 (2006) 22–35.
[36] K. Masuda, T. Ichitsuka, N. Koumura, K. Sato, S. Kobayashi, Tetrahedron 74 (2018) 1705–1730.
[37] T. Yu, J. Jiao, P. Song, W. Nie, C. Yi, Q. Zhang, P. Li, ChemSusChem 13 (2020) 2876–2893.
[38] a) X. Zhuang, J. Liu, S. Zhong, L. Ma, Green Chem. 24 (2022) 271–284;
b) X. Zhuang, J. Liu, Y. Ji, X. Wu, X. Zhang, L. Chen, Q. Zhang, L. Ma, Chem Catalysis (2023) 3;
c) J. Liu, Y. Song, H. Wang, L. Ma, *Green* Chem. Eng. 3 (2022) 64–70.
[39] a) J. Liu, Y. Zhu, C. Wang, T. Singh, N. Wang, Q. Liu, Z. Cui, L. Ma, Green Chem. 22 (2020) 7387–7397;
b J. Liu, Y. Song, X. Zhuang, M. Zhang, L. Ma, Green Chem. 23 (2021) 4604–4617.
[40] S. Mi, L. Chen, X. Zhang, Q. Zhang, L. Ma, J. Liu, RSC Adv. 14 (2024) 16747–16757.
[41] R. Mészáros, B.-J. Peng, S.B. Ötvös, S.-C. Yang, F. Fülöp, ChemPlusChem 84 (2019) 1508–1511.
[42] C. Yue, L. Gu, Z. Zhang, X. Wei, H. Yang, Arab. J. Chem. 15 (2022) 103865.
[43] J. Zhang, A.R. Teixeira, L.T. Kögl, L. Yang, K.F. Jensen, AICHE J. 63 (2017) 4694–4704.
[44] J. Tu, L. Sang, H. Cheng, N. Ai, J. Zhang, Org. Process Res. Dev. 24 (2019) 59–66.
[45] X. Duan, J. Yin, M. Huang, A. Feng, W. Fu, H. Chen, Z. Huang, Y. Ding, J. Zhang, Chem. Eng. Sci. 248 (2022) 117113.
[46] P. Wang, Z. Peng, X. Wang, Y. Lin, H. Hong, F. Chen, X. Chen, J. Zhang, Chem. Eng. Sci. 269 (2023) 118460.
[47] S.P. Bawane, S.B. Sawant, Chem. Eng. J. 103 (2004) 13–19.